HHS Public Access

Author manuscript

Ann Work Expo Health. Author manuscript; available in PMC 2024 February 13.

Published in final edited form as:

Ann Work Expo Health. 2023 February 13; 67(2): 266–280. doi:10.1093/annweh/wxac070.

Characterization of the Emissions and Crystalline Silica Content of Airborne Dust Generated from Grinding Natural and Engineered Stones

Drew Thompson,

Chaolong Qi*

Centers for Disease Control and Prevention, National Institute for Occupational Safety and Health, Division of Field Studies and Engineering, Cincinnati, OH 45226, USA

Abstract

In this study, we systematically characterized the airborne dust generated from grinding engineered and natural stone products using a laboratory testing system designed and operated to collect representative respirable dust samples. Four stone samples tested included two engineered stones consisting of crystalline silica in a polyester resin matrix (formulations differed with Stones A having up to 90wt% crystalline silica and Stone B up to 50wt% crystalline silica), an engineered stone consisting of recycled glass in a cement matrix (Stone C), and a granite. Aerosol samples were collected by respirable dust samplers, total dust samplers, and a Micro-Orifice Uniform Deposit Impactor. Aerosol samples were analyzed by gravimetric analysis and x-ray diffraction to determine dust generation rates, crystalline silica generation rates, and crystalline silica content. Additionally, bulk dust settled on the floor of the testing system was analyzed for crystalline silica content. Real-time particle size distributions were measured using an Aerodynamic Particle Sizer. All stone types generated similar trimodal lognormal number-weighted particle size distributions during grinding with the most prominent mode at an aerodynamic diameter of about 2.0–2.3 μm, suggesting dust formation from grinding different stones is similar. Bulk dust from Stone C contained no crystalline silica. Bulk dust from Stone A, Stone B, and granite contained 60, 23, and 30wt% crystalline silica, respectively. In Stones A and B, the cristobalite form of crystalline silica was more plentiful than the quartz form. Only the quartz form was detected in granite. The bulk dust, respirable dust, and total dust for each stone had comparable amounts of crystalline silica, suggesting that crystalline silica content in the bulk dust could be representative of that in respirable dust generated during grinding. Granite generated more dust per unit volume of material removed than the engineered stones, which all had similar normalized dust generation rates. Stone A had the highest normalized generation rates of crystalline silica, followed by granite, Stone B, and Stone C (no crystalline silica), which likely leads to the same trend of respirable crystalline

*Author to whom correspondence should be addressed: Chaolong Qi; Phone: (001) 513-841-4532; hif1@cdc.gov.

Disclaimer

The findings and conclusions in this report are those of the author(s) and do not necessarily represent the official position of the National Institute for Occupational Safety and Health, Centers for Disease Control and Prevention. Mention of any company or product does not constitute endorsement by the National Institute for Occupational Safety and Health, Centers for Disease Control and Prevention.

Conflicts of Interest

Both authors declare no conflicts of interest.

silica (RCS) exposure when working with these different stones. Manufacturing and adoption of engineered stone products with formulations such as Stone B or Stone C could potentially lower or eliminate RCS exposure risks. Combining all the effects of dust generation rate, size-dependent silica content, and respirable fraction, the highest normalized generation rate of RCS consistently occurs at 3.2–5.6 μm for all the stones containing crystalline silica. Therefore, removing particles in this size range near the generation sources should be prioritized when developing engineering control measures.

Keywords

artificial stone; agglomerated stone; quartz surface; countertop; silicosis

Introduction

Engineered stone has become an increasingly popular countertop option among consumers. However, it can contain more than 90% crystalline silica by mass, about twice that seen in natural granite (Fernández Rodríguez et al., 2013, NIOSH and OSHA, 2015). Because of this high crystalline silica content, workers manufacturing, fabricating, and installing engineered stone countertops may have increased risks of overexposure to respirable crystalline silica (RCS). Silicosis, an untreatable fibrotic disease of the lungs, is an occupational respiratory disease caused by overexposure to RCS (NIOSH, 1986). Recently, outbreaks of silicosis among engineered stones workers have been reported in Israel (Kramer et al., 2012), Spain (Pérez-Alonso et al., 2014), Australia (Hoy et al., 2018), Belgium (Ronsmans et al., 2019), and the U.S. (Rose et al., 2019; Heinzerling, 2020).

In the U.S., the Occupational Health and Safety Administration (OSHA) has set a Permissible Exposure Limit (PEL) for RCS of 0.05 mg m^{-3} as an 8 h time-weighted average (CFR, 2019). Multiple field studies have demonstrated that the dust controls used in some stone countertop workplaces are inadequate at limiting exposure to this level. Phillips et al. (2013) ranked task-specific geometric mean exposures to RCS for a variety of tasks in four stone countertop fabrication shops in the Oklahoma City area of the U.S. The four tasks with the highest estimated exposures were dry sweeping, dry cutting, dry grinding, and dry polishing. All workers who used dry fabrication methods exceeded the PEL, even in cases where the task duration was limited. In a survey of 47 granite countertop fabrication shops in Oklahoma, 15% of shops reported using dry methods for edge grinding most of the time (Phillips and Johnson, 2012). This value is similar to the findings of Glass et al. (2022) where 16% of the 324 participants in the engineered stone fabrication industry in Victoria, Australia spent more than 50% of the time doing dry work in their most recent jobs. Field studies by the U.S. National Institute for Occupational Safety and Health (NIOSH, 2016a; NIOSH, 2016b; NIOSH, 2016c) in relatively large stone countertop fabrication shops found that cutting was mostly performed by machines operated remotely, such as bridge saws or water-jet cutters, but final grinding of the stone edge profiles was exclusively conducted by workers using handheld grinders. Those grinding tasks led to the highest RCS exposure among workers in these shops. The NIOSH studies reported overexposure to RCS for the workers conducting grinding and some polishing tasks in these shops, even

when regular wet methods were employed. A recent NIOSH study (2021) reported that the RCS exposure for workers conducting grinding tasks can be reduced to levels below the OSHA PEL by supplementing the regular wet methods incorporated in the grinders with a sheet-water-wetting method. There is a need for additional or more effective engineering controls to consistently reduce RCS exposures to permissible levels.

Dust and crystalline silica generation rates, dust size distribution, and size-dependent crystalline silica content are valuable information for the selection or development of effective and feasible engineering controls for processes that lead to the highest RCS exposures (Qi et al., 2016). This characterization is best done systematically in a well-controlled laboratory test system. Of the four tasks identified by Phillips et al. (2013) as having the highest estimated RCS exposures, only the cutting and polishing of engineered stone have been characterized in a laboratory using one or more of the metrics highlighted above. To the best of our knowledge, no prior laboratory study has been conducted to characterize the dust generated from grinding engineered stone, which was found to be the task associated with the highest RCS exposure in a NIOSH field study (NIOSH 2016a).

Carrieri et al. (2020) reported the particle size distributions measured by scanning mobility particle spectrometer and optical particle counter from cutting two resin matrix engineered stones, a sintered stone, and granite by an angle grinder equipped with a stone-cutting blade in a laboratory chamber. Crystalline silica content was determined in the respirable dust and bulk dust. Hall et al. (2022) reported the emissions generated from two resin matrix engineered stones, a sintered stone, sandstone, and granite during cutting by an angle grinder equipped with cutting blades and polishing by an angle polisher equipped with polishing paper in a laboratory dust tunnel facility. They measured the particle size distributions via a wide range aerosol spectrometer. Crystalline silica content was measured in the bulk material, inhalable dust, thoracic dust, and respirable dust. In addition, a cascade impactor was used to measure the size-dependent crystalline silica content. Ramkissoon et al. (2022) reported the emissions generated from 12 resin matrix engineered stones, white granite, black granite, and white marble during cutting by an angle grinder equipped with a diamond blade in an enclosed cabinet. They measured particle size distributions by suspending respirable dusts in water and using a dynamic light scattering technique, making it difficult to have direct comparisons to results from aerosol instrumentation in other studies.

Although the laboratory experimental results from in the studies above provided valuable information, the mass concentrations reported by Carrieri et al. (2020) and Hall et al. (2022) are not straightforward to generally estimate real-world RCS exposure or guide engineering control studies. Compared to particle concentrations measured from specific laboratory settings, a generation rate would potentially serve as a better metric to derive real-world RCS exposure of various workplace conditions by modeling with the incorporation of the space dimensions and aerosol dispersion mechanisms.

The aim of this paper is to characterize the dust generated during the dry grinding of engineered and natural stones inside a controlled laboratory testing system by following a standard method to determine dust and crystalline silica generation rates, dust size

distributions, and crystalline silica content. The results obtained will serve as the basis to 1) identify stone products currently available that potentially lower or eliminate RCS exposure, 2) develop potential engineering control measures and, 3) evaluate engineering control effectiveness by comparing the reduced generation rates obtained from the same standard method.

Methods

Natural and engineered stone samples

Four stone materials were investigated in this study: three engineered stones (labeled Stones A, B, and C throughout) and one natural stone, granite. Stones A and B were from the same manufacturer and contained crystalline silica in a polyester resin matrix. Stone A had a manufacturer-claimed crystalline silica content of up to 90%. Stone B was made using a new formula that the manufacturer claimed lowered the crystalline silica content to less than 50%, on par with that seen in most granites. Stone C contained recycled glass in a Portland cement matrix. With glass being amorphous silica, the crystalline silica in Stone C should have been limited to the minute amounts present in the cement matrix. The manufacturer-claimed crystalline silica content was less than 0.2%. The importer of the Granite sample listed an estimated crystalline silica content of up to 72%. To ensure similar contact surfaces between the stone sample's edge and the grinding cup wheel, the thickness of the stone samples was maintained at approximately 30 mm. In some instances, this required clamping several substrates of the same stone together. The manufacturer reported composition of the stone materials, sample dimensions, number of substrates per sample, sample mass, and measured stone material density are summarized for each stone in Table 1.

Laboratory testing system

Stone samples were ground inside a controlled laboratory testing system designed and operated for characterizing the generation rate of respirable dust according to European Standard EN 1093–3 (CEN, 2006). HEPA-filtered air with a flow rate of 0.17 m^3 s^{-1} carried the respirable dust generated from grinding stone samples in an enclosed chamber to a duct containing three sampling ports. See supplementary Figure S1 for a schematic of the laboratory testing system and Qi et al. (2016) for a full description.

A hand-held pneumatic angle grinder (GPW-216, Gison Machinery Co., Ltd., Taiwan) equipped with a 10 cm diameter, coarse, diamond grinding cup wheel (Model SIS-4SPCW-SC, Stone Industrial Supplies, Inc., USA) was manually operated through the chamber's glove ports. In each experimental run, two operators alternated grinding the stone samples for 4 min each. Three runs were completed for each stone material with all but one run having 8 min of active grinding. The second run for Stone C had 16 min of active grinding. Before and after each experimental run, stone samples were weighed on a scale with 5 g certified readability (Model D51XW25WR3, OHAUS Corp., USA) to determine the mass removed during grinding.

Sampling methods

Three isoaxial sampling probes extracted aerosols from the duct of the testing system to (a) up to eight respirable and total dust samplers operated in parallel, (b) an Aerodynamic Particle Sizer (APS) Spectrometer (Model 3321, TSI Inc., USA), and (c) a Micro-Orifice Uniform Deposit Impactor (MOUDI) (Model 110, TSI Inc., USA). The sampling probes were near-isokinetic and estimated to have less than 10% sampling bias for particles smaller than 11 μm. The overall sampling biases of the sampling trains were estimated to be less than 10% for particles with diameters ranging from 5 nm to 9 μm (see supplementary material for more details on the estimation of sampling efficiency).

The MOUDI collected size-classified aerosol samples on 47 mm diameter, 5 μm pore size polyvinyl chloride (PVC) filters acting as impaction substrates and after-filter. Grease or oil was not applied to the MOUDI impaction substrates for the purpose of reducing particle bounce, as their use is unsuitable for the chemical analysis of silica (Chubb and Cauda, 2017). Additional investigation on the effect of particle bounce is beyond the scope of this study but more discussions are covered in the supplementary material. From the MOUDI's size-classified samples, the total dust mass was estimated by summing the mass on all stages. Respirable dust fractions were estimated by multiplying the mass on each stage with the ACGIH criterion for the respirable fraction (Vincent, 2007) at the midpoint aerodynamic diameter of the stage (respirable fraction of 100% and 0% were assumed for the after-filter and inlet stage, respectively) prior to taking the summation of all stages.

GK 4.162 RASCAL Cyclones (Mesa Laboratories, Inc., USA) operated at a flow rate of 9.0 l min^{-1} were used to collect respirable dust on 47 mm diameter, 5 μm pore size PVC filters backed by cellulose support pads in three-piece conductive cassettes following NIOSH Methods 0600 and 7500 (NIOSH, 1998a; NIOSH, 2003). Two RASCALs were employed for each experimental run, except for the first run of Stone C where only one RASCAL was used.

Total dust remaining airborne in the testing system was sampled at a flow rate of 9.0 l min^{-1} onto 47 mm diameter, 5 μm pore size PVC filters backed by cellulose support pads in closed-face, three-piece conductive cassettes. One total dust sample was collected for each experimental run, except for the first and third runs of Stone C where zero and two samples were collected, respectively. As previously noted, and elaborated in the Supplementary Material, the testing system was designed and operated for the transport and sampling of representative respirable dust following European Standard EN 1093–3 (CEN, 2006), as this size fraction is most pertinent for occupational exposures. Total dust, collected to supplement the respirable dust samples, was likely subject to losses during transport and sampling which would result in the total dust collected not being entirely representative of the total dust emitted during grinding. However, because the total dust generated by all stones would be subject to the same losses, relative comparisons are still valid and carry additional values.

After the completion of three experimental runs for each stone, we collected bulk dust samples from the dust settled on the floor of the testing chamber for analysis. Then the testing chamber was thoroughly cleaned to prevent sample cross-contamination.

All PVC filters from the MOUDI, RASCALs, and closed-face cassette samplers were pre-weighed and post-weighed to determine dust mass collected. Crystalline silica analysis of each bulk dust and air sample was performed by x-ray diffraction (XRD) in accordance with NIOSH Method 7500 (NIOSH, 2003) to quantify the amount of quartz, cristobalite, and tridymite forms of crystalline silica present. The PVC filters from all the air samples were processed by muffle furnace ashing for sample preparation. Depending on analytical instruments, analysts, and XRD interferences from feldspar or between silica polymorphs, limits of detection (LOD) were 40–90 μg for dust mass and 5–100 μg, 5 μg, and 10–100 μg for cristobalite, quartz, and tridymite, respectively. In the few cases when masses were below the LOD, the value of $\mathrm{LOD}/\sqrt{2}$, which is often suggested as a substitute with fairly modest bias for non-detectable samples results (Hewett and Ganser, 2007), was substituted for the mass. Note that we did not perform this substitution for tridymite for any stones and cristobalite for Granite because they were not detected in their respective bulk dust samples.

From the mass of the dust and crystalline silica of each sample, we calculated the crystalline silica content and the normalized generation rate. Crystalline silica content was defined as the percent crystalline silica by weight. The normalized generation rate, G, represented the mass of airborne dust or crystalline silica (either respirable, total, or size-classified dust) generated per unit of volume removed from the stone sample during grinding and is defined by Equation 1, where ρ_m is the bulk material density of the stone sample, m_{sampl} is the mass collected by the sampler, m_{remov} is the mass removed from the stone sample, and Q and Q_{sampl} are the nominal flow rates of the test chamber and sampler, respectively.

$$G = \frac{Q\rho_m m_{sampl}}{Q_{sampl} m_{remov}} \qquad \text{Equation 1}$$

Crystalline silica content and normalized generation rate are not measured directly, but instead determined through other quantities via functional relationships. Thus, the combined standard uncertainty for uncorrelated input quantities, as defined in Equation 2, was used to estimate the standard deviation by following the approach of International Organization for Standardization (2008):

$$u_c(y) = \sqrt{\sum_{i=1}^{N} \left(\frac{\partial f}{\partial x_i}\right) u^2(x_i)} \qquad \text{Equation 2}$$

where f is the functional relationship, x_i is the arithmetic mean of mass measurement i (dust, quartz, cristobalite, or tridymite), $u(x_i)$ is the standard uncertainty of mass measurement i, N is the number of mass measurements, and $\partial f / \partial x_i$ is evaluated at x_i.

Welch's analysis of variance (ANOVA) and Welch's unequal variances t-test were performed for the hypothesis testing regarding the crystalline silica content measured by different samplers. The first test used Welch's ANOVA to determine whether, for each stone type, the crystalline silica content collected by individual MOUDI stages had equal means. The second used Welch's t-test to determine whether, for each stone type, the crystalline silica content collected by individual MOUDI stages and that of the total dust from closed-

face cassette samplers had equal means. The third test used Welch's ANOVA to determine whether, for each stone type, the crystalline silica content in samples collected by RASCAL and closed-face cassette samplers and the MOUDI-derived respirable and total dust samples had equal means. In the calculation of p-values, combined standard uncertainty calculated from Equation 2 was used as an estimate of standard deviation. The null hypothesis was rejected for p-values less than 0.05.

The size distributions of particles with aerodynamic diameters ranging from 0.5 to 20 μm were measured every 1 s by the APS. In the Aerosol Instrument Manager (AIM) (v10.2.0.11, TSI Inc., USA) software package the Stokes correction was applied to improve APS sizing accuracy for particles with density greater than 1100 kg m^{-3} (Wang and John, 1987; TSI Incorporated, 2013). In accordance with the work of Marshall et al. (1991), which accounts for the effects of both particle density and shape on APS sizing, the particle density entered in AIM for the Stokes correction was the bulk material density divided by the dynamic shape factor of the particle, ρ_m/χ. The dynamic shape factor χ is a correction to account for particle shape in calculation of drag force. Its value was unknown and found by a least-squares fitting of the respirable mass derived from the APS measurement to the respirable mass collected by the RASCAL samplers (see supplementary material for more details on treatment of APS data).

Number and mass-based particle size distributions representative of the stone grinding process were obtained from the APS. To account for transients due to particle transport in the testing system, the periods of active grinding were identified as those having the highest moving average of particle number concentration over the nominal grinding duration. For each stone material, the particle number and mass distributions were calculated from the APS data collected each second during periods of active grinding. Trimodal lognormal size distribution functions were fit to APS-measured particle number distributions using the procedure outlined in the supplementary material.

Results

Crystalline silica content

The crystalline silica content by percent mass in the size-dependent samples by MOUDI, respirable dust samples by RASCAL, total dust samples from closed-face cassettes, MOUDI-derived respirable and total dust samples, and bulk dust samples are presented in Figure 1 for Granite, Stone A, and Stone B. Stone C is not included in the figure since no crystalline silica was detected, which agrees with the specifications given by the manufacturer. Air samples were subject to size-dependent sampling losses (see supplementary Figure S3 for estimates of these losses). In any case, crystalline silica content is a ratio of masses measured on the same sample, and the sampling losses will have negligible effect on the calculated crystalline silica content since it is realistic to assume that there was no selective sampling loss for crystalline silica.

The quartz form of crystalline silica constituted 30wt% of the bulk dust from Granite, which is within the range listed by the manufacturer and those typically found in granite (NIOSH and OSHA, 2015). The bulk dust from Stone A was found to contain 46wt% cristobalite and

14wt% quartz. The bulk dust from Stone B was 12wt% cristobalite and 11wt% quartz. The manufacturer's claim that Stone B had crystalline silica content comparable to that of natural stone was found to be true. The tridymite form of crystalline silica was not detected in any of the bulk dust samples.

Granite, Stone A, and Stone B had decreasing crystalline silica content, in all forms present, with decreasing particle sizes for aerodynamic diameters smaller than approximately 3 μm. It has been found that for particles smaller than about 1 μm there is a marked decrease in XRD response attributed to the amorphous layer on the surface of the silica particle contributing an appreciable volume percentage of the particle (Stacey et al., 2021; Page, 2003). A particle size-dependent correction factor could be applied to the XRD response to account for this, as done by Hall et al. (2022) for particles collected by a cascade impactor. However, such a correction is not applicable for size-integrated samples, such as those collected by the RASCAL and total dust samplers, so we decided to not perform it to consistently compare the results from MOUDI and size-integrated samplers.

The crystalline silica content for Stones A and B on the first two stages of the MOUDI (> 10 μm) was lower than that of particles with aerodynamic diameters of 1 to 10 μm. It is possible that these larger particles contained less crystalline silica compared to smaller particles. But it is also possible that the lower silica content observed was caused by particle bounce on the first two stages of the MOUDI, as discussed in the supplementary material.

Even though we observed size-dependent variations in crystalline silica content as described above, for each stone, the difference between the mean crystalline silica content collected on each individual MOUDI stage was only statistically significant for Stone A ($p = 0.030$). See supplementary Table S2 for the calculated p-values from this comparison using Welch's ANOVA. For each stone, there was no statistical difference between the mean crystalline silica content on each individual MOUDI stage and that of the total dust samples collect by closed-face cassettes (see Table S3 for the calculated p-values from this comparison using Welch's t-test).

For the crystalline silica content of size-integrated samples, there was excellent agreement between the total dust collected by closed-face cassette and that derived from MOUDI, as seen in Figure 1. The difference between the crystalline silica content in the respirable size fraction from RASCAL and that derived from the MOUDI is slightly larger but to be expected, as there were few MOUDI stages within the steepest portion of the respirable fraction criterion. Another consideration is that the RASCAL cyclone, like any other sampler, is not a perfect representation of the sampling convention. A small bias is to be expected. Altogether, for each stone, there was no statistical difference in crystalline silica content among various size-integrated samples (see supplementary Table S2 for the calculated p-values from this comparison using Welch's ANOVA). From Figure 1, one can see that the crystalline silica content from size-integrated samples were comparable to that seen in the bulk dust.

Normalized generation rates

The size-dependent normalized generation rates of dust and crystalline silica are plotted in Figure 2. Unlike crystalline silica content, sampling losses will affect the normalized generation rate. Sampling losses for the MOUDI were estimated to exceed 10% for particles with aerodynamic diameters greater than 13 μm (see supplementary Figure S3(b)). However, relative comparisons between stones for the first two MOUDI stages are still valid. While differing in magnitude, the normalized generation rates of both dust and crystalline silica for the two engineered stones with a resin matrix, Stones A and B, exhibited similar patterns in size-dependency with the highest rates for particles 5.6–10 μm in aerodynamic diameter. The size-dependent normalized generation rates of dust for the engineered stone with a cement matrix, Stone C, and Granite had similarly shaped distributions with the highest rate for particles larger than 18 μm and a second peak at 5.6–10 μm.

Comparing the results in Figure 1 and 2, the variation of the normalized dust generation rate as a function of particle size was more dominant than that of the silica content. Incorporating the respirable fraction criterion at the midpoint aerodynamic diameter of each MOUDI stage, the size-dependent normalized generation rates of RCS is plotted in Figure 3. The highest normalized generation rate of RCS consistently occurred at 3.2–5.6 μm for all the stones containing crystalline silica.

Figure 4 summarizes the size-integrated normalized generation rates. For the normalized generation rates of respirable and total dust, Granite was the highest while Stones A, B, and C were all comparable. For the normalized generation rate of crystalline silica in both the respirable and total size fractions, Stone A was the highest, followed by Granite, and then Stone B.

Particle size distributions

The number-weighted and mass-weighted particle size distributions measured by the APS during stone grinding, corrected to account for particle density and shape, are plotted in Figure 5. Plotted along with the APS data are the best fit trimodal lognormal distributions (see supplementary Table S1 for the best fit trimodal lognormal distribution parameters). The total number concentration was highest during the grinding of Stone C, followed in decreasing order by Granite, Stone B, and Stone A. In the number-weighted size distributions, all stones had their most prominent mode located at an aerodynamic diameter of about 2.0–2.3 μm, second most prominent mode at 1.0–1.1 μm, and least prominent mode at 5.4–6.9 μm. The trimodal lognormal distributions exhibited an excellent fit with coefficients of determination, R^2, of 0.999 for all stones.

When converting number-weighted size distributions to mass-weighted ones using the Hatch-Choate equation (Hatch and Choate, 1929, Hinds, 1999), a mode at 7.8–8.0 μm is the most prominent as shown in Figure 5b, with two modes at 1.2–1.6 μm and 3.6–5.0 μm contributing to the tail on the left-hand side of the distribution. The mode at 7.8–8.0 μm is also present in the mass-weighted size distributions measured by the MOUDI. See supplementary Figure S5 for a comparison of the average mass-weighted size distributions for the entire duration of the experimental runs as measured by the MOUDI and APS.

Discussion

Using the normalized generation rate as a metric for characterizing the emissions from subtractive processes, such as grinding, sanding, and cutting, enables comparison of emissions from different studies on different tasks and provides valuable input parameters for modeling workplace exposure. Nominal values of concentrations will be dependent on the dilution occurring in the testing system used to generate the data. In contrast, a generation rate obtained by following the European Standard EN 1093–3 (CEN, 2006) will be independent of system dilution rates and allow for comparisons between studies. The normalized generation rate, defined in Equation 1, is the mass of emissions generated per unit of volume removed from the workpiece. The nominal generation rate, typically represented in mass per unit of time, was normalized to include the effect of material removed from the corresponding grinding activity (see supplementary Table S4 for the material removal rates measured in this study). The volume removed from workpieces by grinding might be estimated from geometric measurements and/or countertop design features, such as dimensions of slabs, dimensions of cutouts, radii of corners, edge profiles, etc. With the normalized generation rate, the RCS mass generated by a worker during the full-shift can be derived, which may be readily incorporated into a model to estimate the worker's RCS exposure after considering the aerosol dispersion, background concentration, and other modeling factors. Furthermore, by comparing the normalized generation rate with and without the use of different engineering control measures, the effectiveness of the control measures can be evaluated. Such an approach will allow prompt identification and optimization of feasible control measures in a standard laboratory setting prior to more expensive field validations as was done by a study from NIOSH (2014) on controlling RCS exposures from cutting fiber-cement.

The ranking of the stones studied by their mean normalized generation rates of RCS was, from highest to lowest, Stone A (15.6 mg cm^{-3}), Granite (10.8 mg cm^{-3}), Stone B (6.31 mg cm^{-3}), and Stone C (not detected). For identical amounts of grinding activities, a worker's RCS exposure is likely to be commensurate with the normalized generation rate of RCS for that given stone product. However, it is unclear whether the accelerated silicosis seen in workers exposed to engineered stone dust is a result of overexposure to RCS alone, or if intrinsic material properties of the dust (trace metals, pigments, resins, etc.) potentiate this effect (Mandler et al., 2022). Pavan et al. (2016) reported that the large amount of redox-active transition metal ions and the high content of quartz in the dust from engineered stones with a resin matrix was responsible for the observed strong cell-free oxidative activity in human bronchial epithelial cells and that these dusts were much more reactive when freshly fractured. While Stone C contained no detectable crystalline silica, it did contain a high quantity of recycled glass. To reduce the incidence of silicosis in sandblasters, NIOSH (1998b) identified crushed glass as one of several potential alternative blasting agents to replace silica sand in abrasive blasting. In a study of the comparative pulmonary toxicity of abrasive blasting substitutes and silica sand, Porter et al. (2002) found that the intratracheal instillation of crushed glass in rats produced inflammation and cell damage equivalent to that of silica sand containing 55% crystalline silica. In a 2-week inhalation toxicity study, National Toxicology Program (2020) found that crushed glass was the least toxic of the

four alternatives to silica sand tested, with an absence of induced lung inflammation and proteinosis, but it was the most reactive to the upper respiratory tract, causing microscopic lesions in the nose and larynx. Like quartz (Vallyathan et al., 1995) and engineered stone dust, Ghiazza et al. (2010) reported that the fracturing of vitreous silica, a form of amorphous silica commonly referred to as quartz glass, increased its reactivity, with freshly fractured vitreous silica and quartz inducing similar cytotoxic effects on a macrophage cell line. Recently, Pavan et al. (2020) identified that the local density of a unique family of silanols on the surface of silica dusts is a major determinant of silica particle toxicity. Their findings indicated that these silanols are introduced by surface disorders on silica particles and may be generated by the fracturing of crystalline silica or may be originally present on different sources of amorphous silica. Additional *in vitro* and *in vivo* toxicity studies using the engineered and natural stone dust (both freshly generated and aged) characterized in this and other related studies will be helpful to reveal the overall health effects from the corresponding dust.

Three recent related studies have characterized the emissions from engineered stones with a resin matrix and granite, among other stones, in a controlled environment. Carrieri et al. (2020) and Ramkissoon et al. (2022) investigated stone cutting and Hall et al. (2022) investigated cutting and polishing. All three previous studies found that the crystalline silica content in the respirable dust generated from cutting or polishing of engineered stones with a resin matrix was higher than that for granite. While in the current study this held true for Stone A, Stone B, a product with a new formula to lower crystalline silica content, was verified as having a lower value than that measured in the Granite sample. Similar to that seen by Hall et al. (2022) during stone cutting, we observed that the crystalline silica content of the respirable dust collected during grinding was equivalent to that in the bulk material/dust samples. The crystalline silica content of respirable dust was found to be less than that of the bulk material/dust in the results of Carrieri et al. (2020) for stone cutting and Hall et al. (2022) for stone polishing. Hall et al. (2022) reported that crystalline silica content in each stage of a cascade impactor was consistent with that in the bulk material, except in some cases where the mass collected on the bottom-most stage of impactor approached the LOQ. Although we didn't apply a size-dependent correction factor for XRD response accounting for reduced crystallinity as done in Hall et al. (2022), our results were similar. For each stone, there was no statistically significant difference in the crystalline silica content on any MOUDI stage in comparison with the total dust samples from closed-face cassettes. Qualitatively, the number-weighted size distributions reported here are comparable to the mode measured by Carrieri et al. (2020) in the supermicrometer particle range. The mass-weighted size distributions found in this study fell between those observed during cutting by Carrieri et al. (2020), with a mode between 3 and 10 μm, and by Hall et al. (2022), with modes at 6 and 9 μm. The mass-weighted size distributions measured in this study had larger modes than those measured by Hall et al. (2022) during stone polishing, where the major peak was observed at 0.1 μm and another at 2.5 μm. It is plausible that different fabrication tasks (e.g., cutting, grinding, and polishing) can lead to airborne dust of varying size distributions. Since both particle size and concentration have implications for the RCS exposure profile, the approach used in this study allows better comparison of the RCS exposure profiles among various fabrication tasks and stone types.

Conclusions

During grinding, all stones were found to generate similar trimodal lognormal number-weighted particle size distributions with the most prominent mode located at an aerodynamic diameter of about 2.0–2.3 μm, suggesting that the mechanical process of dust formation from grinding different stones is similar and engineering control measures for the grinding task may be consistently applicable to all stone types. However, the evaluation of the normalized generation rate reveals that 1) Granite generated more dust per unit volume of material removed than Stones A, B, and C, which all had similar normalized dust generation rates; and 2) Stone A had the highest normalized generation rate of crystalline silica, followed by Granite, Stone B, and Stone C (no crystalline silica detected). Therefore, with the same amount of grinding activities and control effectiveness, workers are likely to be exposed to higher RCS when working with Stone A, followed by Granite, Stone B, and, finally, Stone C. Manufacturing and adoption of engineered stone products with formulations such as Stone B or Stone C could potentially lower or eliminate RCS exposure risks.

The crystalline silica content in bulk dust, respirable dust, and total dust for each stone were found to be equivalent for all stones investigated, suggesting that crystalline silica content in the bulk dust could be representative of that in respirable dust generated during grinding. For all the stones containing crystalline silica, the highest normalized generation rate of RCS consistently occurred at 3.2–5.6 μm. When developing engineering control measures, removing particles in this size range near the generation sources should be prioritized to maximize RCS reduction.

Supplementary Material

Refer to Web version on PubMed Central for supplementary material.

Funding

National Institute for Occupational Safety and Health project [Engineering Control of Silica Dust from Stone Countertop Grinding and Polishing (CAN# 927ZLHK)]. This project was supported in part by an appointment to the Research Participation Program at the Centers for Disease Control and Prevention, administered by the Oak Ridge Institute for Science and Education through an interagency agreement between the U.S. Department of Energy and CDC.

Data availability

The data underlying this article will be shared on reasonable request to the corresponding author.

References

Carrieri M, Guzzardo C, Farcas D, Cena LG. (2020) Characterization of Silica Exposure during Manufacturing of Artificial Stone Countertops. Int J Environ Res Public Health; 17: 4489. [PubMed: 32580452]

CEN. (2006) Safety of machinery - Evaluation of the emission of airborne hazardous substances - Part 3: Test bench method for the measurement of the emission rate of a given pollutant, EN 1093–3. Brussels, Belgium: CEN.

CFR. (2019) 29 CFR 1926.1153. CODE OF FEDERAL REGULATIONS. Washington, D.C.: U.S. Government Printing Office, Office of the Federal Register.

Chubb LG, Cauda EG. (2017) Characterizing Particle Size Distributions of Crystalline Silica in Gold Mine Dust. Aerosol Air Qual Res; 17: 24–33. [PubMed: 28217139]

Fernández Rodríguez P, Díaz huerta V, Madera garcía J, Martínez-Blanco D, Blanco JA. (2013) Crystalline Silica in Quartz Agglomerates: A Study of Bulk Materials and an Evaluation of the Respirable Levels in Workplace Atmospheres. In: Harper M, Lee T. (eds.) Silica and Associated Respirable Mineral Particles. West Conshohocken, PA: ASTM International.

Ghiazza M,Polimeni M, Fenoglio I, Gazzano E, Ghigo D, Fubini B. (2010) Does Vitreous Silica Contradict the Toxicity of the Crystalline Silica Paradigm? Chem Res Toxicol; 23: 620–629. [PubMed: 20085295]

Glass DC, Dimitriadis C, Hansen J, Hoy RF, Hore-Lacy F, Sim MR. (2022) Silica Exposure Estimates in Artificial Stone Benchtop Fabrication and Adverse Respiratory Outcomes. Ann Work Expo Health; 66: 5–13. [PubMed: 35015818]

Hall S, Stacey P, Pengelly I, Stagg S, Saunders J, Hambling S. (2022) Characterizing and Comparing Emissions of Dust, Respirable Crystalline Silica, and Volatile Organic Compounds from Natural and Artificial Stones. Ann Work Expo Health; 66: 139–149. [PubMed: 34331440]

Hatch T, Choate SP. (1929) Statistical description of the size properties of non uniform particulate substances. J Franklin Inst; 207: 369–387.

Heinzerling A, Cummings KJ, Flattery J, Weinberg JL, Materna B, Harrison R. (2020) Radiographic Screening Reveals High Burden of Silicosis among Workers at an Engineered Stone Countertop Fabrication Facility in California. Am J Respir Crit Care Med; 203: 764–766.

Hewett P, Ganser GH. (2007) A Comparison of Several Methods for Analyzing Censored Data. Annals Occup Hyg; 51: 611–632.

Hinds WC. (1999) Aerosol technology: properties, behavior, and measurement of airborne particles, New York, NY, John Wiley & Sons, Inc. ISBN 0471194107.

Hoy RF, Baird T, Hammerschlag G, Hart D, Johnson AR, King P, Putt M, Yates DH. (2018) Artificial stone-associated silicosis: a rapidly emerging occupational lung disease. Occup Environl Med; 75: 3.

International Organization for Standardization. (2008) Uncertainty of measurement-Part 3: Guide to the expression of uncertainty in measurement (GUM: 1995). Switzerland: ISO.

Kramer MR, Blanc PD, Fireman E, Amital A, Guber A, Rhahman NA, Shitrit D. (2012) Artificial Stone Silicosis: Disease Resurgence Among Artificial Stone Workers. Chest; 142: 419–424. [PubMed: 22383661]

Mandler WK, Qi C, Qian Y. (2022) Hazardous dusts from the fabrication of countertop: a review. Arch Environ Occup Health; DOI: 10.1080/19338244.2022.2105287.

Marshall IA, Mitchell JP, Griffiths WD. (1991) The behaviour of regular-shaped non-spherical particles in a TSI aerodynamic particle sizer. JAerosol Sci; 22: 73–89.

National Toxicology Program. (2020) NTP Technical Report on the Toxicity Studies of Abrasive Blasting Agents Administered by Inhalation to F344/NTac Rats and Sprague Dawley (Hsd:Sprague Dawley® SD®) Rats. National Toxicology Program, Toxicity Report 91. Research Triangle Park, NC. Available from https://www.ncbi.nlm.nih.gov/books/NBK560066/. Accessed 22 August 2022.

NIOSH. (1986) Occupational respiratory diseases. In: U.S. Department of Health and Human Services, PHS, Centers For Disease Control and Prevention, National Institute for Occupational Safety and Health, DHHS (NIOSH) Publication No. 86–102 (ed.). Cincinnati, OH.

NIOSH. (1998a) Particles not otherwise regulated, respirable: Method 0600 [Online]. NIOSH Manual of Analytical Methods (NMAM®), Issue 3: National Institute for Occupational Safety and Health. Available from: https://www.cdc.gov/niosh/docs/2003-154/pdfs/0600.pdf. Accessed 8 February 2022.

NIOSH. (1998b) Evaluation of substitute materials for silica sand in abrasive blasting. By KTA-Tator, Inc. Contract 200-95-2946R. Available online at https://www.cdc.gov/niosh/topics/silica/abrpt946.html. Accessed 22 August 2022.

NIOSH. (2003) SILICA, CRYSTALLINE, by XRD (filter redeposition): Method 7500 [Online]. NIOSH Manual of Analytical Methods (NMAM®), Issue 4: National Institute for Occupational Safety and Health. Available from: https://www.cdc.gov/niosh/docs/2003-154/pdfs/7500.pdf. Accessed 8 February 2022.

NIOSH. (2014) Comprehensive Report: Evaluation of the dust generation and engineering control for cutting fiber-cement siding. By Qi C, Echt A, Gressel M, Feng HA. EPHB Report No. 358–16a.

NIOSH. (2016a) Evaluation of Crystalline Silica Exposure during Fabrication of Natural and Engineered Stone Countertops. By Zwack LM, Victory KR, Brueck SE, Qi C. HHE Report No. 2014-0215-3250.

NIOSH. (2016b) Engineering Control of Silica Dust from Stone Countertop Fabrication and Installation, In-depth field survey report for the Houston, TX field survey. By Qi C, Echt A. EPHB Report No. 375–11a.

NIOSH. (2016c) Engineering Control of Silica Dust from Stone Countertop Fabrication and Installation, In-depth field survey report for the Mendota Heights, MN field survey. By Qi C, Lo L. EPHB Report No. 375–12a.

NIOSH. (2021) Engineering Control of Silica Dust from Stone Countertop Fabrication and Installation – Evaluation of Wetting Methods for Grinding. By Qi C, Echt A. EPHB Report No. 2021-DFSE-710.

NIOSH, OSHA. (2015) Worker exposure to silica during countertop manufacturing, finishing and installation. National Institute for Occupational Safety and Health,Occupational Safety and Health Administration. DHHS (NIOSH) Publication No. 2015−106, OSHA HA−3768−2015. Available at https://www.osha.gov/sites/default/files/publications/OSHA3768.pdf. Accessed 03 October 2022.

Page SJ. (2003) Comparison of Coal Mine Dust Size Distributions and Calibration Standards for Crystalline Silica Analysis. AIHA J; 64: 30–39.

Pavan C, Polimeni M, Tomatis M, Corazzari I, Turci F, Ghigo D, Fubini B. (2016) Abrasion of Artificial Stones as a New Cause of an Ancient Disease. Physicochemical Features and Cellular Responses. Toxicol Sci; 153: 4–17. [PubMed: 27255382]

Pavan C, Santalucia R, Leinardi R, Fabbiani M, Yakoub Y, Uwambayinema F, Ugliengo P, Tomatis M, Martra G, Turci F, Lison D, Fubini B. (2020) Nearly free surface silanols are the critical molecular moieties that initiate the toxicity of silica particles. Proc Natl Acad Sci USA; 117: 27836–27846. [PubMed: 33097669]

Pérez-Alonso A, Córdoba-Doña JA, Millares-Lorenzo JL, Figueroa-Murillo E, García-Vadillo C, Romero-Morillo J. (2014) Outbreak of silicosis in Spanish quartz conglomerate workers. Int J Occupl Environ Health; 20: 26–32.

Phillips ML, Johnson AC. (2012) Prevalence of Dry Methods in Granite Countertop Fabrication in Oklahoma. J Occup Environ Hyg; 9: 437–442. [PubMed: 22650974]

Phillips ML, Johnson DL, Johnson AC. (2013) Determinants of Respirable Silica Exposure in Stone Countertop Fabrication: A Preliminary Study. J Occup Environ Hyg; 10: 368–373. [PubMed: 23668829]

Porter DW, Hubbs AF, Robinson VA, Battelli LA, Greskevitch M, Barger M, Landsittel D, Jones W, Castranova V. (2002) COMPARATIVE PULMONARY TOXICITY OF BLASTING SAND AND FIVE SUBSTITUTE ABRASIVE BLASTING AGENTS. J Toxicol Environ Health A; 65: 1121–1140. [PubMed: 12167212]

Qi C, Echt A, Gressel MG. (2016) On the Characterization of the Generation Rate and Size-Dependent Crystalline Silica Content of the Dust from Cutting Fiber Cement Siding. Ann Occup Hyg; 60: 220–230. [PubMed: 26391971]

Ramkissoon C, Gaskin S, Thredgold L, Hall T, Rowett S, Gun R. (2022). Characterisation of dust emissions from machined engineered stones to understand the hazard for accelerated silicosis. Sci Rep; 12: 4351. [PubMed: 35288630]

Ronsmans S, Decoster L, Keirsbilck S, Verbeken EK, Nemery B. (2019) Artificial stone-associated silicosis in Belgium. Occup Environ Med; 76: 133. [PubMed: 30385463]

Rose C, Heinzerling A, Patel K, Sack C, Wolff J, Zell-Baran L, Weissman D, Hall E, Sooriash R, Mccarthy RB. (2019) Severe silicosis in engineered stone fabrication workers—California,

Colorado, Texas, and Washington, 2017–2019. MMWR Morb Mortal Wkly Rep; 68: 813. [PubMed: 31557149]

Stacey P, Hall S, Stagg S, Clegg F, Sammon C. (2021) Raman spectroscopy and X-ray diffraction responses when measuring health-related micrometre and nanometre particle size fractions of crystalline quartz and the measurement of quartz in dust samples from the cutting and polishing of natural and artificial stones. J Raman Spectroscopy; 52: 1095–1107.

TSI Incorporated. (2013) Aerosol Instrument Manager® Software for Aerodynamic Particle Sizer® (APS™) Spectrometers. P/N 1930064, Revision H. Shoreview, MN, TSI, Inc.

Vallyathan V, Castranova V, Pack D, Leonard S, Shumaker J, Hubbs AF, Shoemaker DA, Ramsey DM, Pretty JR, McLaurin JL. (1995) Freshly fractured quartz inhalation leads to enhanced lung injury and inflammation. Potential role of free radicals. Am J Respir Crit Care Med; 152: 1003–1009. [PubMed: 7663775]

Vincent JH. (2007). Aerosol sampling : science, standards, instrumentation and applications, Chichester, England, John Wiley & Sons Ltd. ISBN 0470027258.

Wang H-C. John W. (1987) Particle Density Correction for the Aerodynamic Particle Sizer. Aerosol Sci Technol; 6: 191–198.

What's important about this paper?

Outbreaks of silicosis among workers exposed to respirable crystalline silica (RCS) in the engineered stone industry have been reported worldwide. Field studies have identified grinding as the fabrication task linked to the highest exposures of RCS, with overexposure occurring even when traditional dust control methods are employed. This study is the first to use a standard measurement method to systematically characterize dust generation rates during grinding of engineered and natural stone products in a laboratory testing system. The methodology reported herein will allow for standardized comparison of RCS exposure implications associated with different fabrication tasks and provide valuable input parameters for modeling workplace exposures. Furthermore, results from this study identify control strategies to reduce RCS exposures.

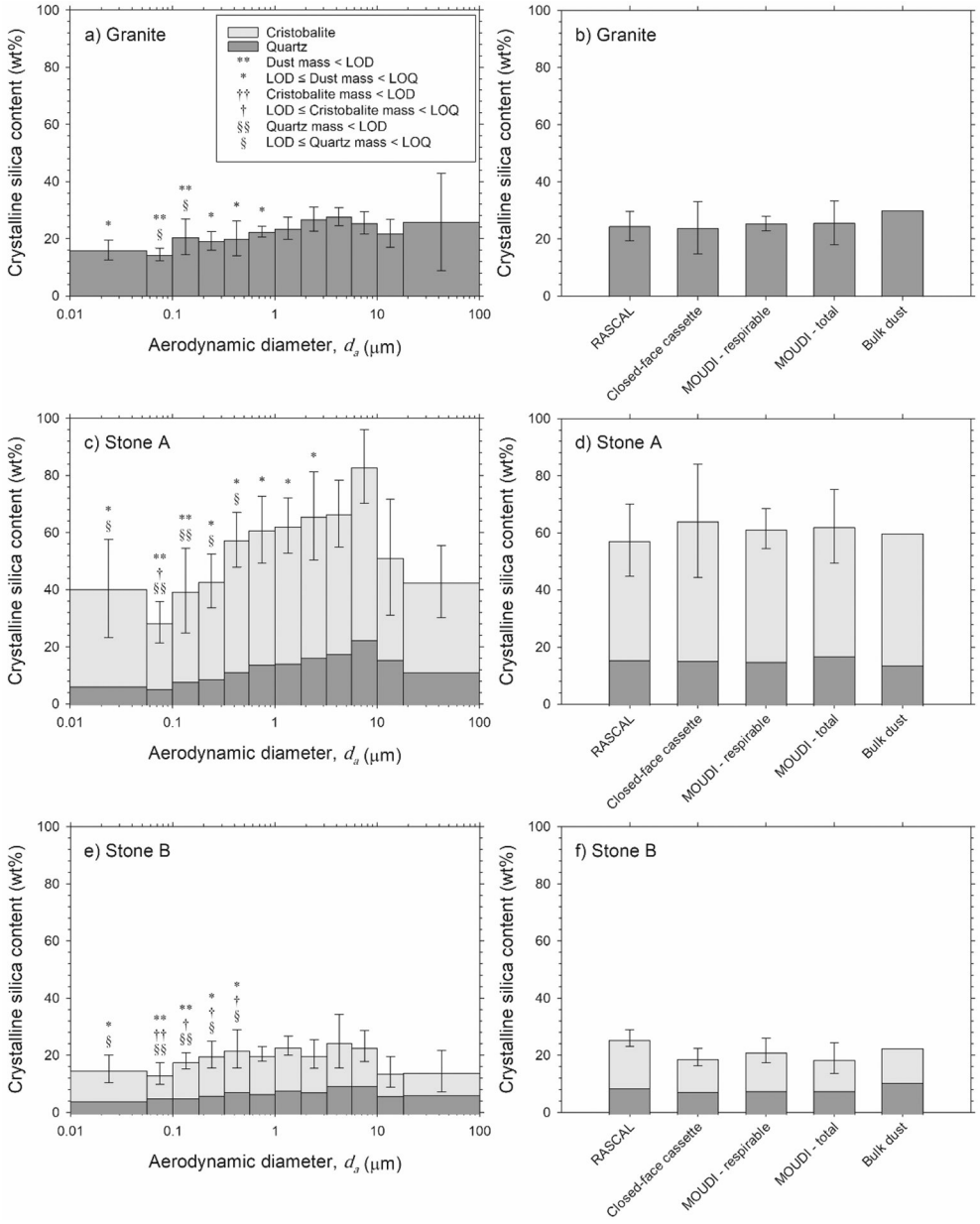

Figure 1.

Crystalline silica content of (a) size-classified Granite dust, (b) size-integrated and bulk Granite dust, (c) size-classified Stone A dust, (d) size-integrated and bulk Stone A dust, (e) size-classified Stone B dust, and (f) size-integrated and bulk Stone B dust. Shadings represent the fraction of cristobalite and quartz forms. Error bars represent the combined standard uncertainty of crystalline silica content. Symbols above the bars indicate whether a mass collected on that stage for one or more replicate sample was below LOD or LOQ (limit of quantification).

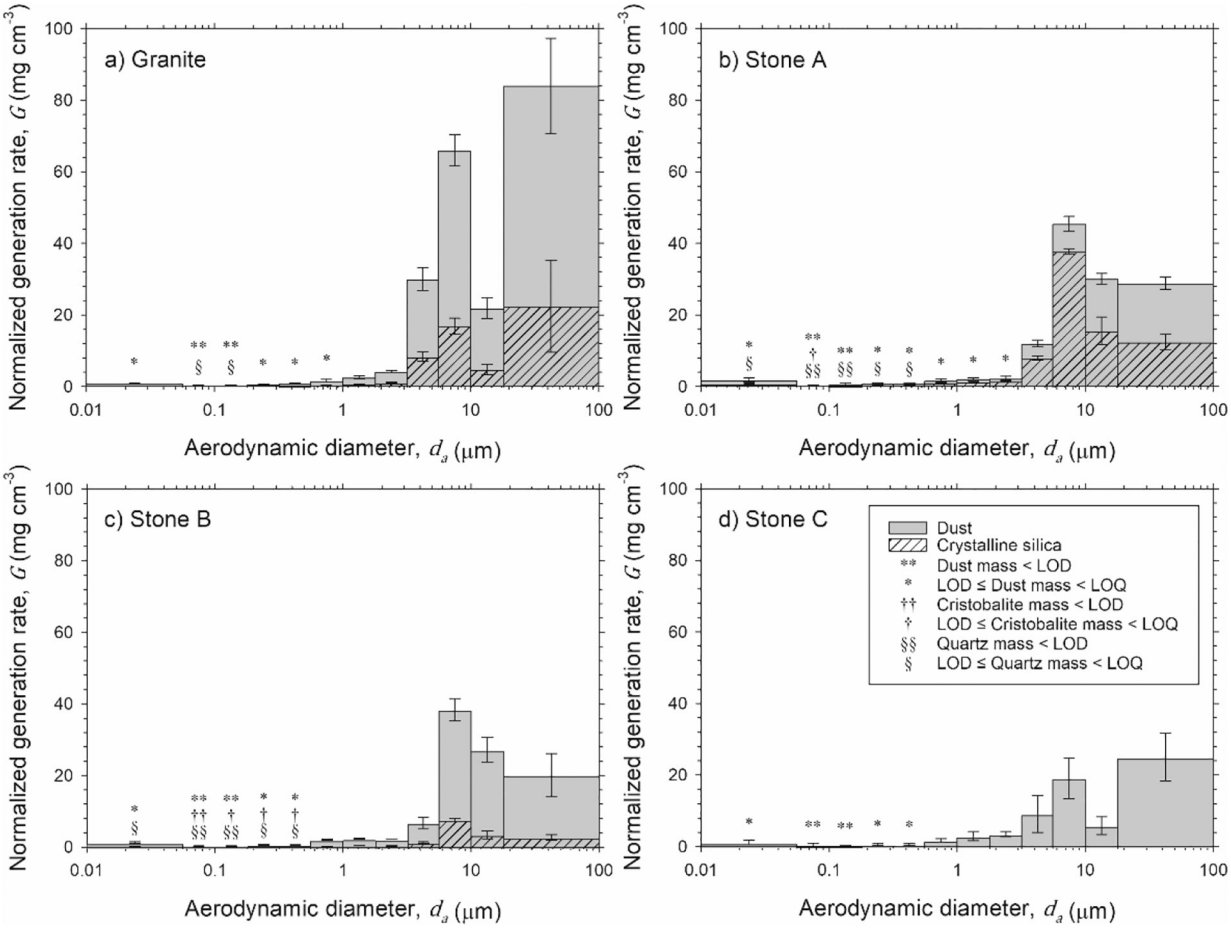

Figure 2.

Size-classified dust and crystalline silica normalized generation rates for the grinding of (a) Granite, (b) Stone A, (c) Stone B, and (d) Stone C. Each data represents the mass of dust or crystalline silica (units of mg) normalized by the volume removed from the stone sample during grinding (units of cm^3). Error bars represent the combined standard uncertainty of the normalized generation rate. Symbols above the bars indicate whether a mass collected on that stage for one or more replicate sample was below LOD or LOQ.

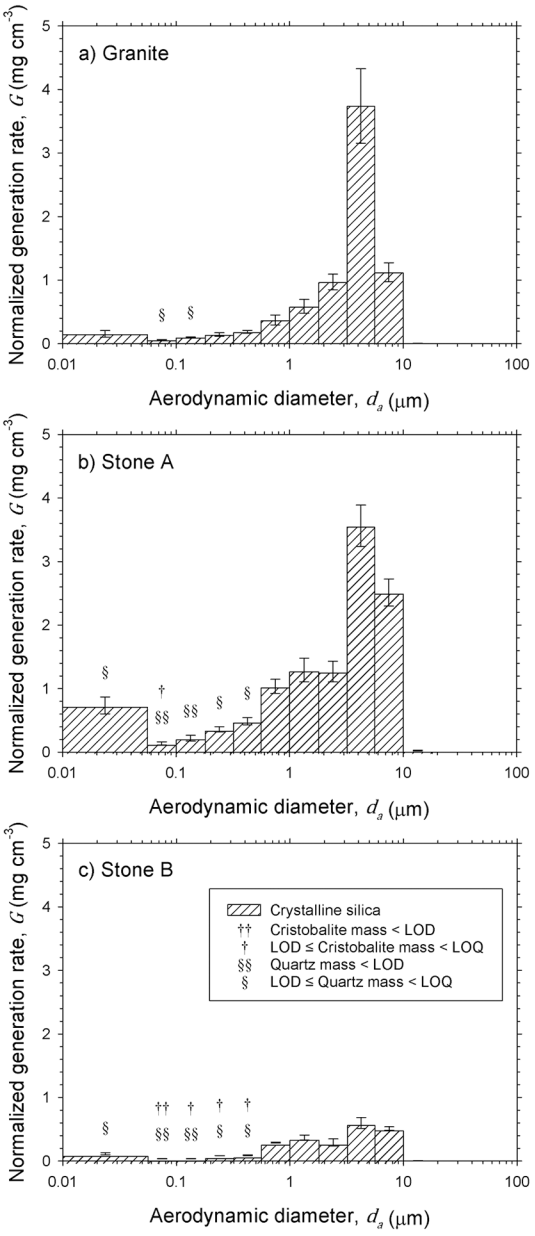

Figure 3.

Size-classified normalized generations rates for RCS from grinding of (a) Granite, (b) Stone A, and (c) Stone B. Each data represents the mass of crystalline silica (units of mg) normalized by the volume removed from the stone sample during grinding (units of cm^3). Error bars represent the combined standard uncertainty of the normalized generation rate. Symbols above the bars indicate whether a mass collected on that stage for one or more replicate sample was below LOD or LOQ.

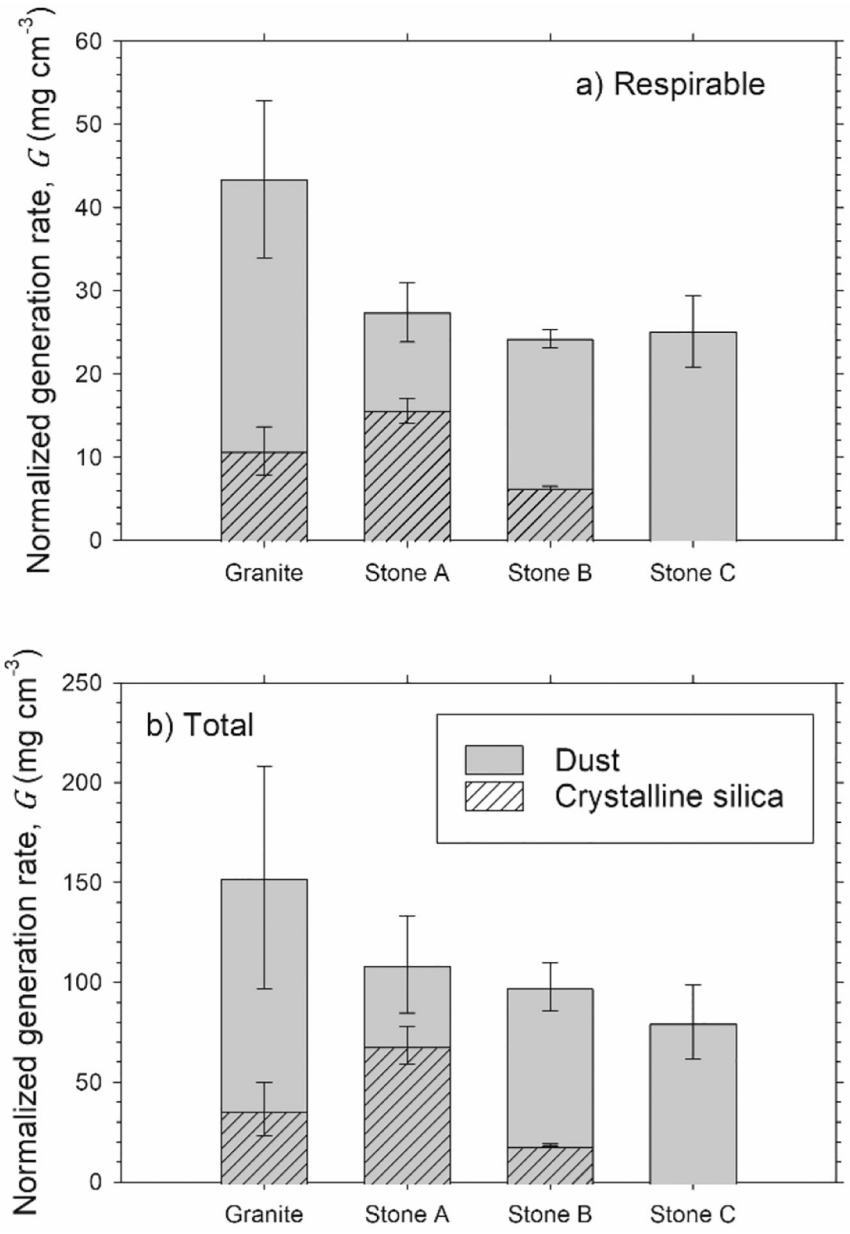

Figure 4.

Dust and crystalline silica normalized generation rates in the (a) respirable and (b) total size fractions. Each data represents the mass of dust or crystalline silica (units of mg) normalized by the volume removed from the stone sample during grinding (units of cm^3). Error bars represent the combined standard uncertainty of the normalized generation rate.

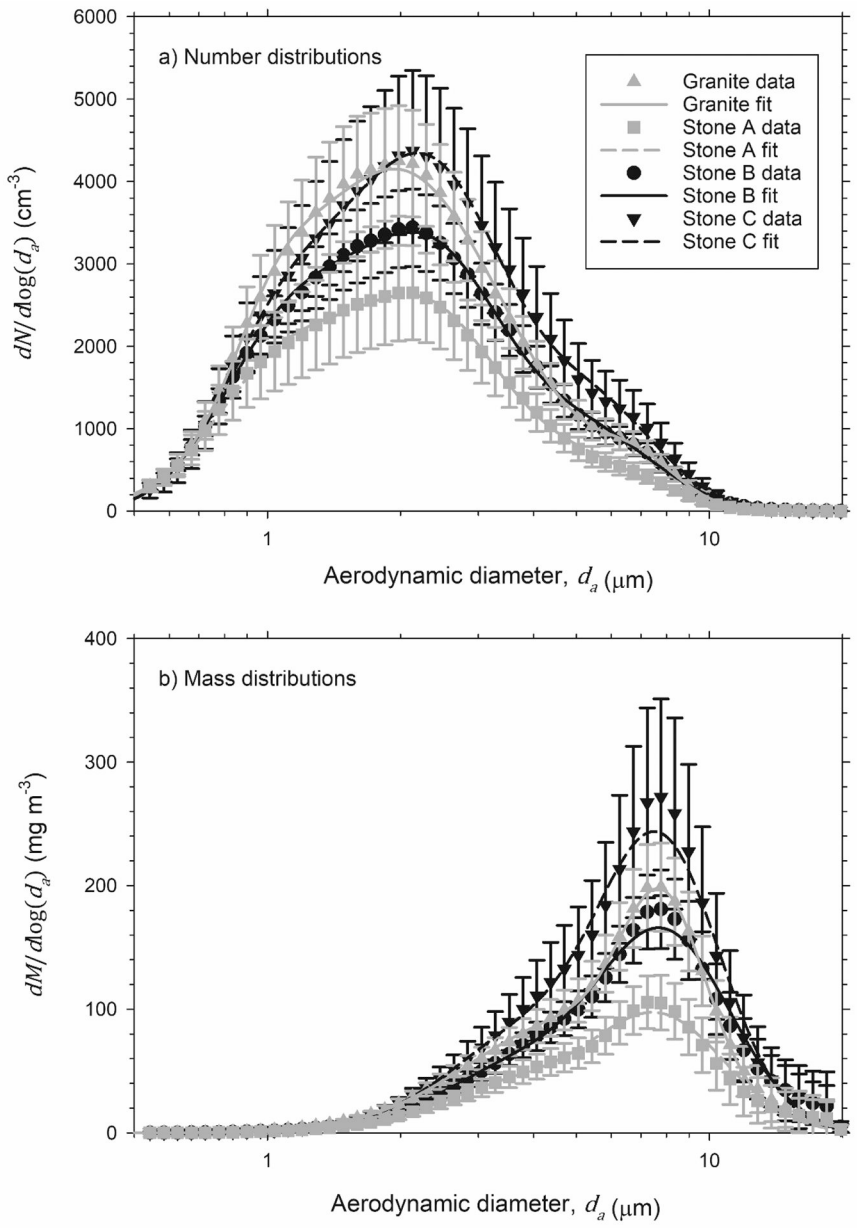

Figure 5.

(a) Number-weighted and (b) mass-weighted particle size distributions of dust generated during grinding of stone samples. Error bars represent the standard deviation. Curves are best fit trimodal lognormal distributions.

Table 1.

Summary of stone sample properties

Stone	Manufacturer reported composition	Stone sample dimensions, L × W × T (mm)	Number of stacked substrates in stone sample	Stone sample mass (kg)	Material density, ρ_m (kg m^{-3})
Granite	Limestone (0–100%); Quartz (0–72%); Feldspar (0–15%); Biotite (0–5%); Iron oxide (0–2%)	310 × 310 × 29	3	6.97	2600
A	Inorganic mineral filler (85–95%), including crystalline silica (70–90%); Polyester resin (5–15%); Pigments and additives (<5%)	200 × 98 × 30	7	1.23	2100
B	Crystalline silica (0–50%) and polyester resin	200 × 97 × 32	7	1.32	2100
C	Post-industrial recycled glass (69%); Portland cement, pigments, and additives (31%)	210 × 200 × 32	1	3.06	2300